The role of post-Golgi transport pathways and sorting motifs in the plasmodesmal targeting of the movement protein (MP) of *Ourmia melon virus* (OuMV)

Natali Ozber[1], Paolo Margaria[2], Charles T. Anderson[1,3], Massimo Turina[4] and Cristina Rosa[1,5]

[1]Plant Biology Graduate Program, Huck Institutes of the Life Sciences, The Pennsylvania State University, University Park, PA 16802, USA

[2]Leibniz-Institut DSMZ - Deutsche Sammlung von Mikroorganismen und Zellkulturen GmbH, Plant Virus Department, 38124 Braunschweig, Germany

[3]Department of Biology, The Pennsylvania State University, University Park, PA 16802, USA

[4]Istituto per la Protezione Sostenibile delle Piante, CNR, Strada delle Cacce 73, 10135, Torino, Italy

[5]Department of Plant Pathology and Environmental Microbiology, The Pennsylvania State University, University Park, PA 16802, USA

Corresponding author: czr2@psu.edu

Running head: Intracellular targeting of OuMV MP

Keywords: vesicle trafficking, tyrosine motif, dileucine motif, trans-Golgi network, plant virus

Summary

Plants have a highly sophisticated endomembrane system that is targeted by plant viruses for cell-to-cell movement. The movement protein (MP) of *Ourmia melon virus* (OuMV) is targeted to plasmodesmata (PD) and forms tubules to facilitate cell-to-cell movement. Despite a number of functionally important regions for correct subcellular localization of OuMV MP has been identified, little is known about the pathways OuMV MP hijacks to reach PD. Here, we demonstrate that OuMV MP localizes to the trans-Golgi network (TGN), but not to the multivesicular body/prevacuolar compartment or Golgi, and carries two putative sorting motifs, a tyrosine (Y) and a dileucine (LL) motif, near its N-terminus. Introducing glycine substitutions in these motifs results in loss of OuMV infectivity in *Nicotiana benthamiana* and Arabidopsis (*Arabidopsis thaliana*). Live cell imaging of GFP-labeled sorting motif mutants shows that Y motif mutants fail to localize to the TGN, plasma membrane, and PD. Mutations in the LL motif do not impair plasma membrane targeting of MP, but affect its ability to associate with callose deposits at PD. Taken together, these data suggest that both Y and LL motifs are indispensable for targeting of OuMV MP to PD and for efficient systemic infection, but show differences in functionality. This study provides new insights into the role of sorting motifs in intracellular targeting of MPs and vesicle trafficking pathways that plant viruses hijack for cell-to-cell movement.

Introduction

Delivery of cargo proteins between distinct locations in the endomembrane system depends on vesicle trafficking. The plant endomembrane system has unique players controlling trafficking pathways to modulate plant-specific cellular functions and environmental responses (reviewed by Fujimoto and Ueda, 2012). The trans-Golgi network (TGN) acts as an early endosome (EE) and a major sorting platform where secretory, endocytic, and vacuolar pathways merge (Viotti et al., 2010). Endocytosed cargoes are received by the TGN and these cargoes are either returned to the plasma membrane or sent to multivesicular bodies (MVBs)/prevacuolar compartments (PVCs), which in plant cells serve as late endosomes (LEs), for vacuolar degradation (reviewed by Fujimoto and Ueda, 2012; Cui et al., 2016).

Heterotetrameric adaptor protein (AP) complexes are key components of protein sorting in endocytic and post-Golgi secretory pathways (reviewed by Canagarajah et al., 2013). Genetic approaches in Arabidopsis have revealed that AP complexes function in hormone signaling (Di Rubbo et al., 2013; Fan et al., 2013; Kansup et al., 2013; Wang et al., 2013), cytokinesis (Teh et al., 2013), gravitropism (Niihama et al. 2009), reproduction (Kim et al., 2013; Yamaoka et al., 2013; Feng et al., 2018), and immunity (Hatsugai et al., 2016). AP1 mediates protein transport from the TGN/EE to the plasma membrane, the cell plate and the vacuole (Park et al., 2013; Teh et al., 2013; Wang et al., 2013). AP2 regulates clathrin-mediated endocytosis (CME) (Bashline et al., 2013; Di Rubbo et al., 2013; Fan et al., 2013; Kim et al., 2013; Yamaoka et al., 2013), whereas AP3 and AP4 function in vacuolar protein sorting (Feraru et al., 2010; Fuji et al., 2016).

AP-dependent protein sorting is mediated most commonly by the recognition of tyrosine (Y), YXXØ and dileucine (LL), [D/E]XXXL[L/I] motifs (where Ø is a bulky hydrophobic residue and X any amino acid) on cargo proteins. In plants, one of the most studied sorting signals is the Y motif. Several cell surface receptors, receptor-like kinases and receptor-like proteins (reviewed by Geldner and Robatzek, 2008), transporters (BOR1; Takano et al., 2010) and vacuolar sorting receptors (Happel et al., 2004; Gershlick et al., 2014; Nishimura et al. 2016) carry Y motifs. There are, however, only a few reports showing the recognition of these signals by AP complexes (Holstein et al., 2002: Happel et al., 2004: Gershlick et al., 2014: Nishimura et al. 2016). LL motifs in plants are far less studied. These motifs are important for sorting of tonoplast proteins (reviewed by Pedrazzini et al., 2013), and in this context, the recognition of a LL motif by AP1, but not AP3, has been reported (Wang et al., 2014). Whether this motif functions in plant endocytic pathways remains to be elucidated.

Viral movement proteins (MPs) are critical for mediating virus movement through plasmodesmata (PD), as the size of virus nucleic acids and virions does not allow for passive intercellular movement. Indeed, localization of viral MPs to PD has been demonstrated, and some MPs can increase the PD size exclusion limit to allow for the passage of viruses into adjacent cells (reviewed by Benitez-Alfonso et al., 2010; Niehl and Henlein, 2011). Viral MPs use various transport strategies to reach PD. One of these strategies is hijacking the host endomembrane system (reviewed by Pitzalis and Heinlein, 2017). MPs of several viruses contain putative Y and LL motifs, but there are only few reports pertaining to the role of these sorting motifs in the targeting of viral MPs

to PD. The MP of *Grapevine fanleaf virus* (GFLV, genus *Nepovirus*) contains putative Y and LL motifs near its N terminus and these motifs are also conserved in MPs of other nepoviruses (Laporte et al., 2003). The triple gene block protein TGB3 of *Poa semilatent virus* (PSLV, genus *Hordeivirus*) harbors a conserved YQDLN motif, which conforms to a Y sorting motif, in the central hydrophilic region that is involved in targeting to the cell periphery (Solovyev et al., 2000). *Potato mop-top virus* (PMTV, genus *Pomovirus*) TGB3 also carries the same motif in its central loop. The disruption of this motif abolishes the localization of PMTV TGB3 to the ER and to motile granules, and the targeting of PMTV TGB3 to plasmodesmata (Haupt et al., 2005; Tilsner et al., 2010). Three Y motifs, YLPL/YGKF/YPKF, are present in *Cauliflower mosaic virus* (CaMV, genus *Caulimovirus*) MP and at least one of the three motifs is required for endosomal localization of MP and for tubule formation. Moreover, CaMV MP directly interacts with Arabidopsis AP2M through the three Y motifs (Carluccio et al., 2014). These Y motifs are, however, dispensable for targeting of CaMV MP to the plasma membrane (Carluccio et al., 2014).

The MP of *Ourmia melon virus* (OuMV), a member of the genus *Ourmiavirus,* forms tubules across the cell wall of epidermal cells of OuMV-infected *N. benthamiana,* and virions are lined up within these tubular structures (Rastgou et al., 2009). Confocal microscopy of green fluorescent protein-tagged OuMV MP (GFP:MPwt) also shows the presence of tubular/punctate structures protruding from the plasma membrane into the extracellular space in *N. benthamiana* and *A. thaliana* (Margaria et al., 2016), as well as the presence of GFP:MP puncta between neighboring cells, co-localizing with callose

deposits at PD (Crivelli et al., 2011; Margaria et al., 2016). Alanine-scanning mutagenesis of conserved amino acids of MPs belonging to the 30KDa family revealed three residues at positions 98, 150 and 169 that are required for targeting of OuMV MP and tubule formation in protoplasts, and important for MP structure (Margaria et al., 2016). It is, however, still unknown which intracellular pathways OuMV MP uses to facilitate cell-to-cell movement of virions. OuMV MP contains two potential internalization and trafficking motifs, one putative Y motif, YDKV (88-91), and one putative LL motif, DPIALI (59–64). In this study, we investigated the involvement of OuMV MP in post-Golgi trafficking pathways, and characterized the individual function of each motif in relation to these pathways by introducing glycine substitutions into critical residues of these motifs and examining localization of mutants by confocal microscopy.

Results

1. OuMV MP is trafficked through post-Golgi transport pathways

We previously investigated the subcellular localization of a OuMV GFP:MPwt fusion in *N. benthamiana* leaf epidermal cells, and demonstrated the presence of fluorescent foci at the cell surface, co-localized with PD (Crivelli et al., 2011; Margaria et al., 2016). Further investigation of the localization of GFP:MPwt, expressed together with RdRp and CP, revealed that GFP:MPwt was associated with peripheral mobile structures (Movie S1). To examine whether OuMV MP localizes to endosomal compartments, we used an endocytic marker, FM4-64, which has been shown to follow endocytic pathways in plants (Dettmer et al., 2006; Geldner et al., 2003; Jaillais et al.,

2006). GFP:MPwt-marked puncta appeared to colocalize with FM4-64 in *N. benthamiana* protoplasts (Fig. 1A). To identify the nature of the endosomal compartments in which the MP resides, we transiently co-expressed mCherry-fused organelle marker proteins (Geldner et al., 2009), VTI12 (a TGN marker; Uemura et al., 2004), and RHA1 (a MVB/PVC marker; Sohn et al., 2003), with GFP:MPwt along with RdRp and CP in *N. benthamiana* leaf epidermal cells. We also applied two well-known inhibitors of vesicle trafficking, brefeldin A (BFA; an ARF GEF inhibitor) and Wortmannin (Wm; a phosphatidylinositol-3 and -4 kinase inhibitor), to these cells to dissect the pathways through which MP is trafficked.

mCherry:VTI12 showed the expected punctate pattern of TGN that overlapped with GFP:MPwt, as shown in Fig. 1B, suggesting that MP is recruited to TGN. While 81-89% of MP co-localized with the TGN marker, the co-localization of TGN marker with MP was 49-68%, suggesting that not all mCherry:VTI12-labeled TGN compartments were occupied by MP. We next examined the effect of BFA on GFP:MPwt at the TGN. It has been previously reported that 5-10 µM concentrations of BFA promote dissociation of TGN into small vesicular compartments in tobacco BY-2 cells (Ito et al., 2017). Hence, we treated *N. benthamiana* leaves expressing both mCherry:VTI12 and GFP:MPwt with 10 *µ*M BFA. Upon BFA treatment, both mCherry:VTI12 and GFP:MPwt dispersed into the cytoplasm. While GFP:MPwt dissociated into smaller punctate structures, some of these structures did not completely co-localize with the TGN marker (Fig 1B, lower panel). When we increased the concentration of BFA to 50 µM, we observed BFA-induced GFP:MPwt aggregates in *N. benthamiana* epidermal cells (not

shown). We hypothesize that formation of these aggregates were associated with the toxicity of BFA rather than direct effect of BFA on the trafficking pathways, and we used the lower concentration in all the further experiments.

To assess whether OuMV MP enters a vacuolar trafficking pathway, we investigated the co-localization of GFP:MPwt with mCherry:RHA1. GFP:MP-labeled intracellular compartments did not co-localize with RHA1-positive MVBs/PVCs (Fig. 1C, upper panel). Treatment with 33 µM Wm, which inhibits protein sorting to the vacuole by inducing homotypic fusion and enlargement of MVBs (Wang et al., 2009; Zheng et al., 2014), resulted in RHA1-positive MVBs/PVCs that appeared as ring-like structures (Fig. 1C, lower panel). These structures were not, however, labeled by GFP:MP (Fig. 1C, lower panel), indicating that MP does not shuttle through the MVB/PVC to the vacuole transport pathway. Unexpectedly, we also observed that the punctate signal of GFP:MP was shifted more toward a diffuse cytoplasmic pattern upon Wm treatment. The meaning of this result is not clear at this point.

Since GFP:MPwt associated with the TGN, we further explored whether the MP puncta were also associated with Golgi bodies by transiently co-expressing GFP:MPwt with Man49:mCherry, a *cis*-Golgi marker (Nelson et al., 2007). As expected, Man49:mCherry displayed a spot-like signal typical of Golgi bodies with a weak signal from the ER; however, the spot-like Golgi signal did not overlap with the punctate signal of GFP:MPwt, indicating that GFP:MPwt structures are distinct from Golgi bodies (Fig. 1D, upper panel) and exclusive to the TGN. We also applied 10 µM BFA to *N. benthamiana* leaves expressing the Golgi marker and GFP:MPwt to further test whether

MP sorts in the conventional secretory pathway. In tobacco, BFA inhibits the secretory pathway and causes redistribution of Golgi bodies into ER (reviewed by Robinson et al., 2008; Langhans et al., 2011). Indeed, treatment with 10 µM BFA caused the Golgi marker to relocate to ER (Fig. 1D, lower panel). While GFP:MP showed a dispersed pattern, similar to that observed with the TGN marker upon BFA treatment (Fig. 1B, lower panel), this pattern did not co-localize with the Golgi marker, suggesting that GFP:MPwt does not enter into the ER-to-Golgi secretory pathway.

2. OuMV MP carries Y and LL motifs, and substitutions into these motifs result in the loss of OuMV infectivity and reduced viral replication

OuMV MP carries one putative Y motif, YDKV (88-91), and one putative LL motif, DPIALI (59–64). To determine whether the Y and LL motifs in OuMV MP are functional, we substituted critical residues of these motifs with glycine and generated five mutants of wild-type MP (MPwt) by site-directed mutagenesis: Y (**G**DK**G**), Y/G (**G**DKV), D (**G**PIA**GG**), D/G (**G**PIALI) and LI/GG (DPIA**GG**), as shown in Fig. 2A. To address possible roles of Y and LL motifs in infectivity of OuMV, the ability of mutants to infect *N. benthamiana* and Arabidopsis (*Arabidopsis thaliana*) was examined using OuMV agroclones carrying the desired mutations. Four out of five OuMV mutants carrying MP_Y, MP_Y/G, MP_D, or MP_LI/GG showed no visible symptoms in local (3 dpi) and systemic (14 dpi) leaves of *N. benthamiana* and Arabidopsis, whereas the OuMV carrying MPwt displayed typical symptoms of leaf chlorosis, curling, and stunted growth (Fig. 2B-C). In Arabidopsis, MP_D/G carrying plants exhibited stunted growth as MPwt, but chlorosis and leaf curling were not observed (Fig. 2B, right panel). Unlike in

Arabidopsis, mutant MP_D/G occasionally caused mosaic symptoms in systemic leaves of *N. benthamiana*, but the overall symptoms were milder than upon infection with wild-type OuMV (Fig. 2C, S1A). Symptoms of OuMV carrying MPwt or MP_D/G in *N. benthamiana* appeared as early as 5 dpi (Fig. S1B) and remained visible during the experimental time frame (14 dpi) (Fig. 2C).

The presence of MP mutants in upper uninoculated leaves of *N. benthamiana* at 14 dpi was tested by western blot analysis; only MPwt and MP_D/G could be detected (Fig. 2D, top panel). To test whether the impaired systemic movement of OuMV mutants was due to a lack of expression of MP mutants at the agroinfiltration sites, we performed western blot analysis of *N. benthamiana* leaf extracts for all constructs at 3 dpi, and all MP variants could be detected (Fig. 2D, bottom panel).

Virion accumulation was also determined in upper uninoculated leaves at 14 dpi by double antibody sandwich enzyme-linked immunosorbent assay (DAS-ELISA) using α-CP antiserum. All mutants, except the one carrying MP_D/G, failed to move systemically in both *N. benthamiana* and Arabidopsis (Table 1). We also analyzed the coding sequence of MP in OuMV mutants by RT-PCR and sequencing of the PCR product to determine whether mutations in Y and LL motifs were reversed, or whether additional mutations were introduced during infection assays. The reversion of MP_D to wild-type was observed only in one Arabidopsis plant (Table 1), where indeed symptoms became systemic (not shown).

Next, we assessed if OuMV carrying MP mutants could potentially inhibit virus replication. Briefly, we co-infiltrated each MP mutant or MPwt along with OuMV RdRP,

CP, and pBin61-GFP and collected samples from the infiltrated leaves at 24 hpi and 48 hpi. GFP signal was monitored at 36 hpi to confirm that all plant cells at the infiltrated areas were infected (Fig. S2). Quantification of RNA1 as proxy for replication was performed by qRT-PCR in all samples. At 24 hpi, all wild-type OuMV expressing samples displayed similar levels of RNA1 and all MP mutant expressing samples showed slightly higher amount of RNA1; however, this difference is not statistically significant, suggesting that all mutant constructs were similarly expressed via agrobacterium transient expression (Fig. S3). While all mutants were able to replicate at high levels at 48 hpi, we observed a 3.5- to 7-fold decrease in the replication of all mutants compared to the wild-type (Fig. 2E). This result suggests that mutations in the Y and LL motifs of OuMV MP have also an effect in virus replication.

3. Y and LL motif MP mutants display changes in subcellular localization over time.

We next examined whether Y and LL motif MP mutants display different intracellular localization patterns over time. To characterize the subcellular distribution of MP mutants, we transiently expressed GFP:MP mutants and GFP:MPwt, as a control, with CP and RdRP in *N. benthamiana* epidermal cells (Fig. S4). Similar to GFP:MPwt (Fig. S4A, left panel), GFP-tagged Y motif MP mutants, GFP:MP_Y and GFP:MP_Y/G, appeared to be distributed in the cytoplasm at 36 hpi and 48 hpi (Fig. S4B-C, left panels) with any noticeable change at 72 hpi (Fig. S4B-C, right panel). Y motif mutants accumulated in transvacuolar strands and in patches at the cell cortex. Puncta that were consistently observed in GFP:MPwt (Movie S2) were no longer

apparent in GFP:MP_Y and GFP:MP_Y/G (Movie S3). Occasionally, a few punctate structures were observed in GFP:MP_Y/G; however, these structures were either stationary or had rather restricted movement (Movie S3). GFP-tagged LL motif MP mutants had a cytoplasmic localization at earlier time points (Fig. S4D-F), with peripheral and cytoplasmic puncta readily observable at 60 hpi, similar to GFP:MPwt (Fig. S4D-F, Movie S4).

4. Mutations in the Y but not in the LL motif impair plasma membrane targeting of MP

To examine whether Y and LL motif MP mutants are targeted to the plasma membrane, we stained *N. benthamiana* protoplasts expressing GFP:MPwt or GFP:MP mutants with FM4-64, a plasma membrane marker. GFP:MPwt showed a continuous signal at the cell periphery and this signal strongly overlapped with FM4-64 (Fig. 3A). The peripheral signal of GFP:MP_Y and GFP:MP_Y/G often did not co-localize with FM4-64 (Fig. 3B-C). A similar pattern was observed in *N. benthamiana* epidermal cells expressing GFP:MP_Y or GFP:MP_Y/G, where the peak of FM4-64 often positioned in between two peaks of the MP mutants, suggesting that plasma membrane localization of GFP:MP_Y and GFP:MP_Y/G followed a different pattern than GFP:MPwt (Fig. S5). Moreover, both mutants exhibited an intense and diffuse cytoplasmic signal.

Similar to GFP:MPwt, the peripheral signal of GFP:MP_D/G overlapped with FM4-64, indicating that GFP:MP_D/G localized to plasma membrane (Fig. 3D). The movement deficient mutant GFP:MP_D also displayed a peripheral signal that co-localized with FM4-64; however, the GFP signal was not evenly distributed along

plasma membrane and accumulated at specific sites (Fig. 3E). GFP:MP_LI/GG had an intermediate pattern between GFP:MP_D and GFP:MP_D/G that was more similar to GFP:MPwt (Fig. 3F).

To investigate these observations, *N. benthamiana* epidermal cells expressing GFP:MPwt or mutants were subjected to plasmolysis. While GFP:MPwt, GFP:MP_D, GFP:MP_D/G and GFP:MP_LI/GG were associated with Hechtian strands that attach the plasma membrane to the cell wall (Fig. 4A, 4D-E), GFP:MP_Y or GFP:MP_Y/G (Fig. 4B-C) did not exhibit the same pattern, as GFP-marked strands were absent from the space between the protoplast and the cell wall (Fig. 4). Plasma membrane localization of GFP:MP_D and GFP:MP_LI/GG suggests that mutations of the LL motif do not impair plasma membrane targeting of MP, but alter uniform distribution of MP along the plasma membrane.

5. Movement deficient LL motif MP mutants failed to localize to PD and form tubules

The punctate localization of the two movement deficient LL motif MP mutants, MP_D and MP_LI/GG, along the cell periphery raises the question of whether these punctate structures are associated with PD. We examined the targeting of MP mutants to PD by staining *N. benthamiana* epidermal cells expressing GFP:MPwt or MP mutants with aniline blue, a callose-specific dye. Consistent with our previous results (Margaria et al., 2016), GFP:MPwt co-localized with callose deposits at PD (Fig. 5A). GFP:MP_D/G, able to support movement, exhibited a similar localization pattern compared to GFP:MPwt and the intensity profile across the PD strongly coaligned with

that of aniline blue (Fig. 5B). Although peripheral punctate structures marked by GFP:MP_D and GFP:MP_LI/GG did not predominantly localize to callose deposits (Fig. 5C-D), GFP:MP_LI/GG labeled structures were in close proximity of PD (Fig. 5D). The quantification of particles labeled by GFP:MPwt or GFP:MP mutants and aniline blue revealed that some of GFP:MP_D and GFP:MP_LI/GG co-localize with callose deposits, but the number of co-localized particles was much lower than that of GFP:MPwt and GFP:MP_D/G (Fig. 5E). The statistical analysis of co-localized particles revealed significant differences between GFP:MPwt or GFP:MP_D/G and movement deficient MP mutants, GFP:MP_D and GFP:MP_LI/GG (Fig. 5F). In contrast, no significant difference between GFP:MPwt and GFP:MP_D/G was observed (Fig. 5F). These results suggest that OuMV movement correlates with the ability of its movement protein to be targeted to PD.

To understand the specific role of LL motif in the plasmodesmal targeting of OuMV MP, N-terminal domain truncated OuMV MP mutants retaining the LL motif, MP_84-first 84 amino acids of MP, and retaining both LL and Y motifs, MP_102-first 102 amino acids of MP, were generated based on predicted secondary structure of MP. We monitored the targeting of MP truncated as described above. Both mutants were, however, unable to reach PD (Fig. S6), suggesting that the presence of the LL motif in a truncated MP variant is not sufficient to support plasmodesmal targeting of MP, and the C-terminal region of MP is also involved in this process. Moreover, MP_102 had noticeably lower expression levels (very close to the background signal) compared to MP_84.

Next, we examined whether MP mutants are able to form tubules. Imaging of protoplasts expressing GFP:MP mutants showed that movement deficient mutant GFP:MP_D does not generate tubule protrusions in the extracellular space as seen for GFP:MPwt and GFP:MP_D/G, supporting the hypothesis that that leucine/isoleucine sites of the LL motif are required for tubule formation between cells (Fig. 6). Results for all mutants are summarized in Table 3.

6. AP2M is not required for systemic infection and does not directly interact with MP

Given that CaMV MP hijacks clathrin-mediated endocytosis by directly interacting with the μ subunit of Arabidopsis AP2 (AP2M) through its three Y motifs (Carluccio et al., 2014), we also investigated the possible role of AP2M in the transport of OuMV MP. We first infected Arabidopsis Col-0 (wt), AP2M knockout mutant *ap2m-1* and AP2M-YFP complementation plants with OuMV by mechanical inoculation. There were no obvious differences in symptoms or changes in the number of infected plants among the *ap2m-1* mutant, the complementation line and wild-type (Col-0) at 14 dpi, indicating that the absence of AP2M does not impair systemic infection of OuMV (Table 2).

To investigate whether OuMV MP physically interacts with AP2M, we tested the interaction between the C-terminal μ-homology domain of AP2M (AP2M-MHD) with OuMV MP by a pull-down assay. His-CesA1 has been previously reported as AP2M-MHD interacting protein (Bashline et al., 2013) and was used a positive control in the pull-down assay. Even though the positive control clearly bound AP2M-MHD, we were

unable to detect binding of AP2M with MP *in vitro* (Fig. 7). As opposed to CaMV MP, OuMV MP does not directly interact with AP2M under tested conditions.

Discussion

In this study, we investigated the intracellular trafficking of OuMV MP in the context of post-Golgi transport routes, and the function of Y and LL sorting motifs. Despite the complexity of plant protein sorting arising from the fact that TGN acts as the main sorting hub for Golgi-derived cargoes and internalized cargoes from the plasma membrane, we were able to partially unravel the trafficking routes that OuMV MP hijacks by using organelle markers in combination with inhibitors of vesicle trafficking. TGN localization of OuMV MP, together with its co-localization with FM4-64 stained compartments, demonstrates that OuMV MP trafficks in endosomal pathways (Fig. 1, A-B). Co-localization of endosomal compartments and MPs of other viruses has been reported before (Haupt et al., 2005; Carluccio et al., 2014); however, this is the first study showing that a viral MP resides in the TGN, extending knowledge of the involvement of post-Golgi trafficking pathways in virus movement. We also showed that the canonical secretory pathway is not involved in the transport of OuMV MP since the MP did not co-localize with the Golgi in the absence or presence of BFA (Fig. 1D). Moreover, the redistribution of OuMV MP into the same smaller vesicles as the TGN marker upon low dose BFA treatment suggests that MP exhibits BFA sensitivity only at the TGN, but not at the Golgi. Dependence on the canonical secretory pathway varies between plant viruses (reviewed by Pitzalis and Heinlein, 2017). Whereas the secretory pathway is not involved in targeting of the *Cowpea mosaic virus* (CPMV, genus

Comovirus) MP to the cell periphery (Pouwels et al., 2002), a functional secretory pathway is necessary for the correct localization of the MPs of *Grapevine fanleaf virus* (GFLV, genus *Nepovirus*; Laporte et al., 2003), *Chinese wheat mosaic virus* (CWMV, genus *Furovirus*; Andika et al., 2013), *Potato leafroll virus* (PLRV, genus *Polerovirus*; Genoves et al., 2010) and *Melon necrotic spot virus* (MNSV, genus *Carmovirus*; Vogel et al., 2007). In addition, OuMV MP was not associated with MVBs/PVCs in the absence or presence of Wm (Fig. 1C), confirming that MP trafficks in the first stages of vesicular trafficking, but not in MVB/PVC-to-vacuole pathway, in contrast to CaMV MP (Carluccio et al., 2014) and PTMV TGB2 (Haupt et al., 2005), which co-localize with ARA7-positive MVBs/PVCs. Although OuMV MP showed sensitivity to Wm, this response was different from that of MVBs/PVCs. Based on the finding that OuMV MP localizes to the TGN and does not enter either in the canonical secretory or MVB/PVC-to-vacuole pathways, we hypothesize that MP constitutively cycles between the plasma membrane and the TGN.

Glycine substitutions in the Y motif altered the intracellular distribution of MP. A key question emerging from this observation is whether the Y motif in OuMV MP is a functional internalization motif. Y motifs are recognized by μ-subunits of APs 1-4 (Bonifacino and Traub, 2003). In plants, CME of plasma membrane proteins depends on Y motifs in their cytoplasmic domains to be recognized by AP2M (Di Rubbo et al., 2013; Fan et al., 2013; Kim et al., 2013; Yamaoka et al., 2013) and it has been previously shown that CaMV MP is able to bind Arabidopsis AP2*μ* through three Y motifs (Carluccio et al., 2014). Unlike CaMV MP, we failed to see direct binding of

AP2M to OuMV MP *in vitro* (Fig. 7). Additionally, we did not observe any changes in the infectivity of OuMV in the absence of AP2M in Arabidopsis (Table 2). It is, however, known that AP2M is not the sole regulator of CME in plants; a CME adaptor complex, TPLATE complex (TPC), is involved in the initiation of CME and is thus crucial for recruitment of clathrin and AP2 (Gadeyne et al., 2014). Moreover, AP2 subunits are considered to form partially active complexes in the absence of single subunits (Wang et al., 2016). Hence, other AP2 subunits and/or TPC may be important for internalization of OuMV MP, and in turn for infectivity of OuMV. At this point, we do not have enough evidence that the internalization of OuMV MP directly depends on AP2M. In this context, the Y motif may have other functions such as acting as an intracellular retention signal or maintaining correct protein conformation. In animal viruses for instance, Y motifs in viral glycoproteins have been reported to function as intracellular retention signals (reviewed in Ujike and Taguchi et al., 2015). Replacing the tyrosine residue in YXXI motif of surface protein of *Transmissible gastroenteritis virus* (TGEV, genus *Alphacoronavirus*) abolished intracellular retention of the protein (Winter et al., 2008). Similarly, substituting the tyrosine residue in YTTF motif of the spike protein (S) of *Infectious bronchitis virus* (IBV, genus *Gammacoronavirus*) caused the S protein to localize to the plasma membrane (Schwegmann-Wessels et al., 2004). Another possible scenario is that glycine substitutions into the Y motif of OuMV MP may induce conformational changes, leading to masking of the plasma membrane targeting signal. In PSLV and PMTV, the Y motif is required for the delivery of viral proteins to the cell periphery and PD, but this motif is important for conformation of the protein, rather than

its internalization. In fact, membrane topology analysis of PMTV TGB3 revealed that YQDLN motif resides in ER lumen (Tilsner et al., 2010). We previously identified three amino acid residues (98, 150 and 169) within the core region of OuMV MP (63-206), which are responsible for localization of MP at the cell periphery, and these residues are possibly involved in the correct folding/function of OuMV MP (Margaria et al., 2016). The Y motif of OuMV MP is also located in the core region of the MP, suggesting that it might have a structural role, similar to the one seen for PSLV TGB3 and PMTV TGB3.

OuMV MP has the classical [D/E]XXXL[L/I] sorting motif in which an acidic amino acid is located at the -4th position relative to the first leucine. Replacing the aspartic acid with glycine in DPAILI does not affect the localization of the MP and the resulting mutant behaves similar to the wild-type virus (Fig. S4E, Fig. 3-4D; Fig. 5B; Fig 6, middle panel). Conversely, substitutions of leucine and isoleucine with a pair of glycine residues impair the transport of the OuMV MP to PD. In mammals and yeast, LL motifs are recognized by APs 1-3 with a combination of two subunits: AP1 γ-σ1, AP2 α-σ2, and AP3 δ-σ3 hemicomplexes (Janvier et al., 2003; Doray et al., 2007). The acidic amino acid is not as crucial as dileucine residues for binding to AP2 (Kelly et al., 2008). The binding specificity of plant AP complexes has yet to be elucidated. Only one study has explored direct binding of a canonical LL motif to subunits of AP complexes. The dileucine motif of Arabidopsis tonoplast-localized ion transporter VTI1, EKQTLL, interacts with AP1 γ1/2 and σ1/2 subunits, but not with AP3 δ and σ (Wang et al., 2014), raising the possibility that these subunits could be interacting partners of OuMV MP instead of AP2M. Although we cannot exclude the possibility that the LL motif may be important for

binding of other proteins, our study addresses the function of this motif in the intracellular targeting of OuMV MP.

Previous studies have shown that viral proteins traffic in endocytic and vacuolar pathways (Haupt et al., 2005; Lewis and Lazarowitz, 2010; Carluccio et al., 2014). Our results support the hypothesis that plant viral proteins take advantage of post-Golgi trafficking pathways to facilitate cell-to-cell movement, and provide new insights into these pathways. Based on our findings, we propose the following model (Fig. 8): OuMV MP is targeted to the plasma membrane through a mechanism that is independent of the conventional secretory pathway, similarly to MPs of many other viruses (reviewed by Pitzalis and Heinlein, 2017). While MPs of some viruses reach the plasma membrane and PD by moving along the ER we do not have evidence at this point that OuMV MP follows this model. Once OuMV MP reaches the plasma membrane, it is endocytosed, sorted into the TGN and then recycled back to the plasma membrane, bypassing the MVB/PVC-to-vacuole pathway, to maintain its presence at the plasma membrane and to reach PD. The retrieval of MP from the plasma membrane is possibly AP2M-independent and does not depend on the Y motif (AP2M binding site). On the other hand, the plasmodesmal targeting of MP relies on the LL motif, potentially through its function in endocytic pathways. The precise molecular mechanism of MP targeting is, however, still unknown. In fact, the N-terminal region of MP retaining the LL motif does not act as a plasmodesmal targeting, as opposed to the TMV MP, in which the first 50 amino acid residues were characterized as a plasmodesmal localization signal (Yuan et al., 2016). Moreover, the C-terminus of OuMV has a predicted disordered region with

many potential phosphorylation sites (not shown) that may be important for its regulation and interaction with host proteins. Although this model requires further examination to understand the mechanistic details of the targeting of OuMV MP to PD, to the best of our knowledge, this is the first study showing the role of a LL motif in plasmodesmal targeting of MPs. Movement proteins are often associated to the sites of viral replication, thus it is extremely hard to untangle if a disturbance in viral replication, as the one seen with our mutants, is due to mislocalization of the viral MP from the site of replication, or to modifications of the sites of replication. Our present efforts focus on identifying host factors that are directly involved in post-Golgi trafficking of OuMV MP and cell-to-cell movement of OuMV, to better elucidate the molecular mechanism of the virus movement. Simple viral systems, such as the one presented by OuMV, are an invaluable tool that can be advantageously used to identify missing components of highly complex plant trafficking pathways.

Experimental Procedures

Plant material and growth conditions

N. benthamiana plants were grown in a growth chamber set at 25°C with a 16 h photoperiod, and used at 4-5 weeks old. *Arabidopsis thaliana* seeds were surface sterilized using 50% bleach solution for 5 minutes, rinsed five times with sterile distilled water and plated on ½ MS plates containing 1% agar. Ten-day old seedlings were transferred to soil, grown in a growth chamber at 22 °C, 60% relative humidity, and at a light intensity of 120 μmol/m^{2}s^1 at a 10 h photoperiod, and used when 4-5 weeks old.

Arabidopsis thaliana ecotype Col-0 was used for infectivity assays (as described below). The AP2M knockout mutant *ap2m-1* (SALK_083693) and AP2M-YFP complementation line (Bashline et al., 2013) were provided by Dr. Ying Gu (The Pennsylvania State University, University Park, PA, USA) and genotyped for homozygosity using the primers in Table S1.

Plasmid constructions and *Agrobacterium*-mediated transient expression in plant leaves

The OuMV infectious clone, consisting of the three plasmids pGC-RNA1 (RdRP), pGC-RNA2 (MP) and pGC-RNA3 (CP), and GFP:MP plasmid has been previously described (Crivelli et al., 2011; Margaria et al., 2016). Mutations were inserted into MP and GFP:MP plasmid with the QuickChange Site-Directed Mutagenesis Kit (Stratagene, La Jolla, CA, USA) using primers in Table S1.

The Golgi marker, Man49:mCherry (CD3-967; Nelson et al., 2007), the TGN marker, mCherry:VTI12 (CD3-781541; Geldner et al., 2009), and the MVB/PVC marker, mCherry:RHA1 (CD3-781597; Geldner et al., 2009) were obtained from ABRC (http://www.arabidopsis.org/). The fragments of Ubq10pro::mCherry::VTI12 and Ubq10pro::mCherry::RHA1 were amplified from the original plasmids using the primers in Table S1, and inserted into XhoI/SpeI-digested pORE O2 (CD3-921; Coutu et al., 2007). All plasmids were transformed into *A. tumefaciens* strain C58C1.

A. tumefaciens cultures carrying the desired plasmids were grown in a shaking incubator at 28°C in 2xYT medium supplemented with 50 μg/ml kanamycin and 5 μg/mL tetracycline. Cultures were pelleted when at an optical density at 600 nm (OD600) of 1.0

and resuspended in agroinfiltration buffer (10 mM MES, 10 mM MgCl2 and 100 μM acetosyringone). Bacterial suspensions were generated by mixing the desired combinations at a final optical density at 600 nm (OD600) of 0.2 and 0.05 for GFP:MP/RdRP/CP and the organelle markers respectively. The mixtures were incubated at room temperature for 2 h in the dark and infiltrated on the abaxial side of fully expanded leaves using a needleless syringe.

Infectivity assays, ELISA and RT-PCR

Viral infections were started either from agroinfiltration of a mix of *Agrobacterium* cultures carrying the three plasmids mentioned above or by mechanical inoculation, using sap obtained by grinding virus-infected, fresh *N. benthamiana* tissue in 0.05 M phosphate buffer supplemented with carborundum and silica powders (Margaria et al., 2016). Six *N. benthamiana* and 12 Arabidopsis plants were used for infectivity assays. Double antibody sandwich-enzyme linked immunosorbent assay (DAS-ELISA) was performed as previously described (Margaria et al., 2016). Leaves were sampled for ELISA testing at 14 dpi. Experiments were repeated three times.

RNA extraction and RT-PCR were performed as described in Margaria et al., 2016. Total RNA (100 ng) was used for RT-PCR, and full-length coding sequence of MP was amplified using primers listed in Table S1.

Replication assay

The effect of specific amino acid substitutions in MP on virus replication was measured by agroinfiltrating local leaves with pGC-RNA2 (MP) or mutants, together with pGC-RNA1 (RdRP), pGC-RNA3 (CP), and pBin61-GFP at an OD600 of 1.0. The GFP

signal at the infiltrated sites was monitored at 36 hpi to confirm that agroinfiltrated areas were saturated. Two leaf spots from 3 leaves were pooled for each sample at 24 hpi and 48 hpi. The virus accumulation was measured by quantifying RNA1 by qPCR using primers listed in Table S1. The qPCR was performed in duplicates using iTaq™ Universal SYBR® Green Supermix (BioRad) and a CFX96 (BioRad), following the manufacturer's instructions. The $2^{-\Delta\Delta CT}$ method was used to asses fold changes in replication of wild-type and mutants. The data was normalized first using 18S ribosomal RNA, and then a wild-type control at 24 hpi showing the lowest expression. Four plants were used for qPCR analysis. Statistical analysis was performed using ANOVA.

Protoplast isolation from infected leaves

Protoplasts were prepared from leaves of *N. benthamiana* expressing GFP:MPwt or GFP:MP mutants (together with RdRP and CP) at 66 hpi. Leaf sections were cut into small fragments (~1 cm^2) using a razor blade and incubated in the enzyme solution on a rotor shaker for 6 h at room temperature, as previously described (Margaria et al., 2016).

Plasmolysis, inhibitor and staining experiments

Plasmolysis experiments were carried out by treating *N. benthamiana* leaf sections expressing GFP:MP or mutants, together with RdRP and CP, with 1 M mannitol for 45 min. The leaf sections were imaged at 62 – 66 hpi.

N. benthamiana leaves were infiltrated with 10 µM BFA (stock: 10mg/ml in DMSO; MilliporeSigma St. Louis, MO, USA) or 33 µM Wortmannin (stock: 10 mM in DMSO; MilliporeSigma). Equivalent amounts of DMSO were used as controls. Leaf

samples were imaged after 1 h of the indicated treatment, as described below. *N. benthamiana* protoplasts and epidermal cells were stained with the dye FM4-64 (Thermo Fisher Scientific, Rockford, IL, USA) at a final concentration of 10 µM (stock: 1 mM in water) for 5-15 min. For cell wall staining, *N. benthamiana* leaves were infiltrated with 10 *µ*g/ml propidium iodide solution (stock: 1 mg/ml in water; Thermo Fisher Scientific) and incubated for 30 min. For staining callose deposits, *N. benthamiana* leaves were infiltrated with aniline blue (MilliporeSigma) at a final concentration of 0.1% (stock: 1% (v/w) in 50 mM potassium phosphate buffer, pH 9.0) and incubated for 30 min. All experiments were repeated at least twice.

Confocal microscopy and quantification

Leaf sections or protoplasts were mounted on a microscope slide (Thermo Fisher Scientific) covered with a #1.5 coverslip (Corning, Corning, NY, USA). For confocal microscopy, images were acquired with a Zeiss Cell Observer SD microscope equipped with a Yokogawa CSU-X1 spinning disk head and Plan-Apochromat 63X/NA 1.4 and 40X/NA 1.3, and an Olympus Fluoview (FV) 1000 microscope with a Plan-Apochromat 40X/NA 1.15 water immersion and 60X/NA 1.4 oil immersion objectives. A 543-nm excitation laser line and an emission bandpass filter 585 – 660 nm (Olympus FV1000) were used for imaging of FM-4-64. PI was imaged using a 561 nm excitation laser line with an emission bandpass filter 581 – 654 nm (Zeiss Cell Observer SD). GFP:MPwt was detected using a 488-nm excitation laser with an emission bandpass filter 500 – 530 nm (Olympus FV1000) or 500– 550 nm (Zeiss Cell Observer SD), and aniline blue was imaged using 405-nm excitation laser with an emission bandpass filter 425 – 475

nm (Olympus FV1000 and Zeiss Cell Observer SD). Z-stacks of optical sections were collected at 0.2 µm intervals for time-dependent subcellular localization experiment and at 0.5 µm intervals for the rest of experiments. Images were analyzed and processed using ImageJ (http://imagej.nih.gov/ij) and Adobe Photoshop CC 2017. All images were assembled in Adobe Illustrator CC 2017.

Callose deposits were quantified using the ComDet v.0.4.1 plugin in ImageJ. The particle detection was performed by setting particle size to 2 pixels. For co-localization experiments, maximum distance between spots was adjusted to 2 pixels. Images for quantification were randomly selected. Statistical analysis was performed using ANOVA.

Protein purification

The coding sequence of OuMV MP was cloned into in pMAL-c4x (NEB New England Biolabs), in frame with MBP. MBP-MP was expressed in BL21 (DE3) and the expression was induced with 0.3 mM IPTG for 2 h at 37° C. The pellets were resuspended with amylose column buffer (20 mM Tris-HCl pH7.5, 0.2 M NaCl, 1 mM EDTA) supplemented with 1X Halt protease inhibitor cocktail (Thermo Fisher Scientific) and sonicated five times for 10 sec. The soluble fraction of MBP-MP was applied to pre-equilibrated amylose agarose resin (NEB). After washing the column three times with amylose column buffer, MBP-MP was eluted with five fractions of amylose column buffer supplemented with 30 mM maltose. The fraction containing the highest amount of MBP-MP was concentrated using an Amicon Ultra-15 Centrifugal Filter Unit with

Ultracel- 50kDa(MilliporeSigma, St. Louis, MO, USA) and stored in storage buffer (20 mM Hepes pH 7.5, 5 mM MgCl, 1 mM EDTA, 1 mM DTT, 20% Glycerol).

pGEX-4T2 and pMAL-c4x were kindly provided by Dr. Gitta Coaker (University of California-Davis, CA, USA). GST-AP2M-MHD in BL21Star-pLysS and His-CesA1 in BL21-CodonPlus (DE3)-RIPL were provided by Dr. Ying Gu (The Pennsylvania State University, University Park, PA, USA). GST, GST-AP2M-MHD, and His-CesA1 were expressed and purified as described in Bashline et al., 2013.

Pull-down assay

The soluble fraction of GST and GST-AP2M-MHD was applied to 20 µl of GST-Trap_A (ChromoTek, Hauppauge, NY, USA) pre-equilibrated with extraction buffer (10 mM Tris pH 7.5, 150 mM NaCl, 0.5 mM EDTA) and incubated for 1 h at 4°C. Resin-bound GST or GST-AP2M-MHD were washed five times with extraction buffer and two times with interaction buffer (20 mM Hepes pH 7.5, 5 mM MgCl, 1 mM EDTA, 1 mM DTT). His-CesA1 or MBP-MP was added to GST and GST-AP2M-MHD bound resins, and incubated for 2 h at 4°C. After washing five times with interaction buffer, bound proteins were eluted with 100 μL of 2x SDS-PAGE sample buffer at 60°C for 20 min. The eluted proteins were analyzed by immunoblot against GST, 6xHis-tag, and MP.

Protein extraction, SDS–PAGE, immunoblotting

Leaf sections were collected from agroinfiltrated leaves and upper uninoculated leaves, and homogenized in 2x SDS-PAGE buffer. Extracted proteins were separated in SDS polyacrylamide gels (4% stacking gel, 10% separation gel; Laemmli and Favre, 1973). The proteins were transferred to PVDF membranes (MilliporeSigma) for western

blot analysis. OuMV MP was detected using a non-commercial anti-MP (A314) antiserum as described in Rastgou et al., 2009, followed by incubation with an anti-rabbit horseradish peroxidase (HRP)-conjugated secondary antibody (NXA931; MilliporeSigma) diluted 1:20000 (v/v). GST and 6xHis tag were detected by an HRP-conjugated anti-GST (RPN1236; GE Healthcare, Piscataway, NJ, USA) polyclonal antibody at a dilution of 1:5000 (v/v) and an HRP-conjugated 6x-His epitope tag polyclonal antibody (PA1-983B-HRP; Thermo Fisher Scientific) at a dilution of 1:1000 respectively. SuperSignal™ West Femto Maximum Sensitivity Substrate (Thermo Fisher Scientific) was used for detecting HRP.

Acknowledgements

This work was supported by USDA HATCH Accession No: 1009992, Project No. PEN04604 to C. Rosa and a grant of Penn State College of Agricultural Sciences to N. Ozber. We thank Benjamin Knollenberg (Penn State) for helping with cloning of OuMV MP into pMAL-c4x. Authors have no conflict of interest, financial or otherwise.

References

Andika, I. B., Zheng, S., Tan, Z., Sun, L., Kondo, H., Zhou, X. and Chen, J. (2013) Endoplasmic reticulum export and vesicle formation of the movement protein of Chinese wheat mosaic virus are regulated by two transmembrane domains and depend on the secretory pathway. Virology 435(2):493-503.

Bashline, L., Li, S., Anderson, C.T., Lei, L. and Gu, Y. (2013) The endocytosis of cellulose synthase in Arabidopsis is dependent on μ2, a clathrin-mediated endocytosis adaptin. Plant Physiol 163(1):150–160.

Benitez-Alfonso, Y., Faulkner, C., Ritzenthaler, C. and Maule, A.J. (2010) Plasmodesmata: gateways to local and systemic virus infection. Molecular Plant-Microbe Interactions 23(11):1403–1412.

Bonifacino, J.S. and Traub, L.M. (2003) Signals for sorting of transmembrane proteins to endosomes and lysosomes. Annu. Rev. Biochem. 72:395–447.

Canagarajah, B.J., Ren, X., Bonifacino, J.S. and, Hurley, J.H. (2013). The clathrin adaptor complexes as a paradigm for membrane-associated allostery. Protein Sci. 22: 517-529

Carluccio, A.V., Zicca, S. and, Stavolone, L. (2014) Hitching a Ride on Vesicles: Cauliflower Mosaic Virus Movement Protein Trafficking in the Endomembrane System. Plant Physiol. 164:1261–1270.

Coutu, C., Brandle, J., Brown, D., Brown, K., Miki, B., Simmonds, J. and Hegedus, D.D. (2007) pORE: a modular binary vector series suited for both monocot and dicot plant transformation. Transgenic Res. 16:771– 781.

Crivelli, G., Ciuffo, M., Genre, A., Masenga, V. and Turina, M. (2011) Reverse genetic analysis of Ourmiaviruses reveals the nucleolar localization of the coat protein in *Nicotiana benthamiana* and unusual requirements for virion formation. Journal of Virology 85:5091–5104.

Cui, Y., Shen, J., Gao, C., Zhuang, X., Wang, J., and Jiang, L. (2016). Biogenesis of plant prevacuolar multivesicular bodies. Mol. Plant 9:774–786.

Dettmer, J., Hong-Hermesdorf, A., Stierhof, Y. D., and Schumacher, K. (2006). Vacuolar H+-ATPase activity is required for endocytic and secretory trafficking in Arabidopsis. Plant Cell 18:715–730.

Di Rubbo, S., Irani, N.G., Kim S.Y., Xu Z.Y., Gadeyne A., Dejonghe W., Vanhoutte I., Persiau G., Eeckhout D., Simon S. (2013) The clathrin adaptor complex AP-2 mediates endocytosis of brassinosteroid insensitive1 in Arabidopsis. Plant Cell 25, 2986–2997.

Doray, B., Lee, I., Knisely, J., Bu, G. and Kornfeld, S. (2007) The gamma/sigma1 and alpha/sigma2 hemicomplexes of clathrin adaptors AP-1 and AP-2 harbor the dileucine recognition site. Mol. Biol. Cell. 18:1887-1896.

Fan, L., Hao, H., Xue, Y., Zhang, L., Song, K., Ding, Z., Botella, M.A., Wang, H. and Lin, J. (2013) Dynamic analysis of Arabidopsis AP2 σ subunit reveals a key role in clathrin-mediated endocytosis and plant development. Development 140:3826–3837

Feng, Q.N., Liang, X., Li, S. and Zhang, Y. (2018) The ADAPTOR PROTEIN-3 Complex Mediates Pollen Tube Growth by Coordinating Vacuolar Targeting and Organization. Plant Physiol. 177:216-225.

Feraru, E., Paciorek, T., Feraru, M.I., Zwiewka, M., De Groodt, R., De Rycke, R., Kleine-Vehn, J. and Friml, J. (2010) The AP-3 β adaptin mediates the biogenesis and function of lytic vacuoles in *Arabidopsis*. Plant Cell 22:2812–2824.

Fuji, K., Shirakawa, M., Shimono, Y., Kunieda, T., Fukao, Y., Koumoto, Y., Takahashi, H., Hara-Nishimura, I. and Shimada, T. (2016) The adaptor complex AP-4 regulates vacuolar protein sorting at the trans-Golgi network by interacting with VACUOLAR SORTING RECEPTOR1. Plant Physiology 170:211 – 219.

Fujimoto, M. and Ueda, T. (2012) Conserved and plant-unique mechanisms regulating plant post-Golgi traffic, Front. Plant Sci. 3:197.

Gadeyne, A., Sánchez-Rodríguez, C., Vanneste, S., Di Rubbo, S., Zauber, H., Vanneste, K., Van Leene, J., De Winne, N., Eeckhout, D., Persiau, G., et al. (2014) The TPLATE adaptor complex drives clathrin-mediated endocytosis in plants. Cell 156:691–704.

Geldner, N., and Robatzek, S. 2008. Plant receptors go endosomal: A moving view on signal transduction. Plant Physiol. 147:1565-1574.

Geldner, N., Anders, N., Wolters, H., Keicher, J., Kornberger, W., Muller, P., Delbarre, A., Ueda, T., Nakano, A., and Jürgens, G. (2003). The Arabidopsis GNOM ARF-GEF mediates endosomal recycling, auxin transport, and auxin-dependent plant growth. Cell 112:219–230.

Geldner, N., Dénervaud-Tendon, V., Hyman, D.L., Mayer, U., Stierhof, Y.D. and Chory, J. (2009) Combinatorial analysis of membrane compartments in intact plants with a multicolor marker set. Plant J. 59:169–178.

Genovés, A., Navarro, J. A and Pallás, V. (2010) The intra- and intercellular movement of Melon necrotic spot virus (MNSV) depends on an active secretory pathway. Molecular Plant-Microbe Interactions 23:263–272.

Gershlick, D.C., Lousa, Cde.M., Foresti, O., Lee, A.J., Pereira, E.A., daSilva, L.L., Bottanelli, F., and Denecke, J. (2014). Golgi-dependent transport of vacuolar sorting receptors is regulated by COPII, AP1, and AP4 protein complexes in tobacco. Plant Cell 26:1308–1329.

Happel, N., Honing, S., Neuhaus, J.M., Paris, N., Robinson, D.G. and Holstein, S.E. (2004) Arabidopsis mu A-adaptin interacts with the tyrosine motif of the vacuolar sorting receptor VSR-PS1. Plant J 37:678–693.

Haupt, S., Cowan, G. H., Ziegler, A., Roberts, A. G., Oparka, K. J. and Torrance, L. (2005) Two plant–viral movement proteins traffic in the endocytic recycling pathway. The Plant Cell 17:164-181.

Hatsugai N, Hillmer R, Yamaoka S, Hara-Nishimura I, Katagiri F. (2016) The μ Subunit of Arabidopsis Adaptor Protein-2 Is Involved in Effector-Triggered Immunity Mediated by Membrane-Localized Resistance Proteins. Mol Plant Microbe Interact 29:345–351

Holstein, S.E. (2002) Clathrin and plant endocytosis. Traffic 3:614-620.

Ito, Y., Toyooka, K., Fujimoto, M., Ueda, T., Uemura, T. and, Nakano, A. (2017) The trans-Golgi network and the Golgi stacks behave independently during regeneration after brefeldin A treatment in tobacco BY-2 cells. Plant Cell Physiol 58:811–821.

Jaillais, Y., Fobis-Loisy, I., Miege, C., Rollin, C. and Gaude, T. (2006) AtSNX1 defines an endosome for auxin-carrier trafficking in Arabidopsis. Nature 443:106–109.

Janvier, K., Kato, Y., Boehm, M., Rose, J. R., Martina, J. A., Kim, B. Y., Venkatesan, S. and Bonifacino, J. S. (2003) Recognition of dileucine sorting signals from HIV-1 Nef and LIMP-II by the AP-1 gamma-sigma1 and AP-3 delta-sigma3 hemicomplexes J. Cell Biol. 163:1281–1290.

Kansup, J., Tsugama, D., Liu, S. and Takano, T. (2013) The Arabidopsis adaptor protein AP-3*μ* interacts with the G-protein β subunit AGB1 and is involved in abscisic acid regulation of germination and post-germination development, Journal of Experimental Botany 64(18):5611–5621.

Kelly, B.T., McCoy, A.J., Spate, K., Miller, S.E., Evans, P.R., Honing, S., and Owen, D.J. (2008) A structural explanation for the binding of endocytic dileucine motifs by the AP2 complex. Nature 456:976–979.

Kim, S.Y., Xu, Z.Y., Song, K., Kim, D.H., Kang, H., Reichardt, I., Sohn, E.J., Friml, J., Juergens, G. and, Hwang, I. (2013) Adaptor protein complex 2-mediated endocytosis is crucial for male reproductive organ development in Arabidopsis. Plant Cell 25:2970–2985.

Langhans, M., Förster, S., Helmchen, G., and Robinson, D. G. (2011). Differential effects of the brefeldin A analogue (6R)-hydroxy-BFA in tobacco and Arabidopsis. J. Exp. Bot. 62:2949–2957.

Laporte, C., Vetter, G., Loudes, A. M., Robinson, D. G., Hillmer, S., Stussi-Garaud, C. and Ritzenthaler, C. (2003) Involvement of the secretory pathway and the cytoskeleton in intracellular targeting and tubule assembly of Grapevine fanleaf virus movement protein in tobacco BY-2 cells. The Plant Cell 15:2058-2075.

Lewis, J.D. and Lazarowitz, S.G. (2010) Arabidopsis synaptotagmin SYTA regulates endocytosis and virus movement protein cell-to-cell transport. Proc Natl Acad Sci USA 107:2491–2496.

Margaria, P., Anderson, C. T., Turina, M. and Rosa, C. (2016) Identification of Ourmiavirus 30K movement protein amino acid residues involved in symptomatology, viral movement, subcellular localization and tubule formation. Molecular Plant Pathology 17:1063-1079.

Nelson, B.K., Cai, X. and Nebenführ, A. (2007) A multi-color set of in vivo organelle markers for colocalization studies in Arabidopsis and other plants. The Plant Journal 51:1126-1136.

Niehl, A. and Heinlein, M. (2011) Cellular pathways for viral transport through plasmodesmata. Protoplasma 248:75–99.

Niihama, M., Takemoto, N., Hashiguchi, Y., Tasaka, M. and, Morita, M.T. (2009) ZIP genes encode proteins involved in membrane trafficking of the TGN-PVC/vacuoles. Plant Cell Physiol 50:2057–2068.

Nishimura, K., Matsunami, E., Yoshida, S., Kohata, S., Yamauchi, J., Jisaka, M., Nagaya, T., Yokota, K. and Nakagawa, T. (2016) The tyrosine-sorting motif of the vacuolar sorting receptor VSR4 from Arabidopsis thaliana, which is involved in the interaction between VSR4 and AP1M2, μ1-adaptin type 2 of clathrin adaptor complex 1 subunits, participates in the post-Golgi sorting of VSR4. Biosci. Biotechnol. Biochem. 80:694-705.

Park, M., Song, K., Reichardt, I., Kim, H., Mayer, U., Stierhof, Y.D., Hwang, I. and Jürgens, G. (2013) *Arabidopsis* μ-adaptin subunit AP1M of adaptor protein complex 1

mediates late secretory and vacuolar traffic and is required for growth. Proc. Natl Acad. Sci. USA 110(10):318–323.

Pedrazzini, E., Komarova, N.Y., Rentsch, D., and Vitale, A. (2013) Traffic routes and signals for the tonoplast. Traffic 14:622–628.

Pitzalis, N. and Heinlein, M. (2017) The roles of membranes and associated cytoskeleton in plant virus replication and cell-to-cell movement. J Exp Bot. 69:117-13.

Pouwels, J., Van der Krogt, G.N.M., Van Lent, J., Bisseling, T. and Wellink J. (2002) The cytoskeleton and the secretory pathway are not involved in targeting the cowpea mosaic virus movement protein to the cell periphery. Virology 297:48-56.

Rastgou, M., Habibi, M. K., Izadpanah, K., Masenga, V., Milne, R. G., Wolf, Y. I., Koonin E. V. and Turina, M. (2009) Molecular characterization of the plant virus genus Ourmiavirus and evidence of inter-kingdom reassortment of viral genome segments as its possible route of origin. Journal of General Virology 90:2525-2535.

Robinson, D. G., Langhans, M., Saint-Jore-Dupas, C., and Hawes, C. (2008) BFA effects are tissue and not just plant specific. Trends Plant Sci. 13:405–408.

Schwegmann-Wessels, C., M. Al Falah, D. Escors, Z. Wang, G. Zimmer, H. Deng, L. Enjuanes, H. Y. Naim, and G. Herrler. (2004) A novel sorting signal for intracellular localization is present in the S protein of a porcine coronavirus but absent from severe acute respiratory syndrome-associated coronavirus. J. Biol. Chem. 279**:**43661-43666.

Sohn, E.J., Kim, E.S., Zhao, M., Kim, S.J., Kim, H., Kim, Y.W., Lee, Y.J., Hillmer, S., Sohn, U., Jiang, L. and Hwang, I. (2003). Rha1, an Arabidopsis Rab5 homolog, plays a critical role in the vacuolar trafficking of soluble cargo proteins. The Plant Cell 15:1057–1070.

Solovyev, A.G., Stroganova, T.A., Zamyatnin, J., Fedorkin, O.N., Schiemann, J. and Morozov, S.Yu. (2000) Subcellular sorting of small membrane-associated triple gene block proteins: TGBp3-assisted targeting of TGBp2. Virology 269:113–127.

Takano, J., Tanaka, M., Toyoda, A., Miwa, K., Kasai, K., Fuji, K., Onouchi, H., Naito, S. and Fujiwara, T. (2010). Polar localization and degradation of Arabidopsis boron transporters through distinct trafficking pathways. Proc. Natl. Acad. Sci. USA 107:5220–5225.

Teh, O.K., Shimono, Y., Shirakawa, M., Fukao, Y., Tamura, K., Shimada, T. and Hara Nishimura, I. (2013) The AP-1 *μ* adaptin is required for KNOLLE localization at the cell plate to mediate cytokinesis in *Arabidopsis*. Plant Cell Physiol. 54:838–847.

Tilsner J., Cowan G.H., Roberts A.G., Chapman S.N., Ziegler A., Savenkov E. and Torrance L. (2010) Plasmodesmal targeting and intercellular movement of potato mop-top pomovirus is mediated by a membrane anchored tyrosine motif on the lumenal side of the endoplasmic reticulum and the C-terminal transmembrane domain in the TGB3 movement protein. Virology 402:41-51.

Uemura, T., Ueda, T., Ohniwa, R.L., Nakano, A., Takeyasu, K. and Sato, M.H. (2004) Systematic analysis of SNARE molecules in Arabidopsis: dissection of the post-Golgi network in plant cells. Cell Struct Funct. 29:49–65.

Ujike, M. and Taguchi, F. (2015) Incorporation of spike and membrane glycoproteins into coronavirus virions. Viruses 7:1700–1725.

Viotti, C., Bubeck, J., Stierhof, Y.D., Krebs, M., Langhans, M., van den Berg, W., van Dongen, W., Richter, S., Geldner N., Takano, J., Jürgens G., de Vries, S.C., Robinson, D.G. and Schumacher, K. (2010) Endocytic and Secretory Traffic in Arabidopsis Merge in the Trans-Golgi Network/Early Endosome, an Independent and Highly Dynamic Organelle. Plant Cell 22:1344–1357.

Vogel, F., Hofius, D. and Sonnewald, U. (2007) Intracellular trafficking of potato leafroll virus movement protein in transgenic arabidopsis. Traffic 8:1205-1214.

Wang C., Hu T., Yan X., Meng T., Wang Y., Wang Q., et al. (2016) Differential regulation of clathrin and its adaptor proteins during membrane recruitment for endocytosis. Plant Physiol. 171:215–229.

Wang, X., Cai, Y., Wang, H., Zeng, Y., Zhuang, X., Li, B., Jiang, L. (2014) Trans-Golgi network-located AP1 gamma adaptins mediate dileucine motif-directed vacuolar targeting in Arabidopsis. Plant Cell 26:4102–4118.

Wang, J., Cai, Y., Miao, Y., Lam, S.K. and Jiang, L. (2009) Wortmannin induces homotypic fusion of plant prevacuolar compartments. Journal of Experimental Botany 60:3075–3083.

Wang, J.G., Li, S., Zhao, X.Y., Zhou, L.Z., Huang, G.Q., Feng, C. and Zhang, Y. (2013) HAPLESS13, the *Arabidopsis* μ1 adaptin, is essential for protein sorting at the trans-Golgi network/early endosome. Plant Physiol. 162:1897–1910.

Winter, C., Schwegmann-Wessels, C., Neumann, U. and Herrler, G. (2008) The spike protein of infectious bronchitis virus is retained intracellularly by a tyrosine motif. J. Virol. 82**:**2765-2771.

Yamaoka, S., Shimono, Y., Shirakawa, M., Fukao, Y., Kawase, T., Hatsugai, N., Tamura, K., Shimada, T. and, Hara-Nishimura, I. (2013) Identification and dynamics of

Arabidopsis adaptor protein-2 complex and its involvement in floral organ development. Plant Cell 25:2958–2969.

Yuan, C., Lazarowitz, S.G., Citovsky, V. (2016) Identification of a functional plasmodesmal
localization signal in a plant viral cell-to-cell-movement protein. mBio 7:e02052-15.

Zheng, J., Han, S.W., Rodriguez-Welsh, M.F. and Rojas-Pierce, M. (2014) Homotypic vacuole fusion requires VTI11 and is regulated by phosphoinositides. Molecular Plant 7: 1026–1040.

Figure 1.

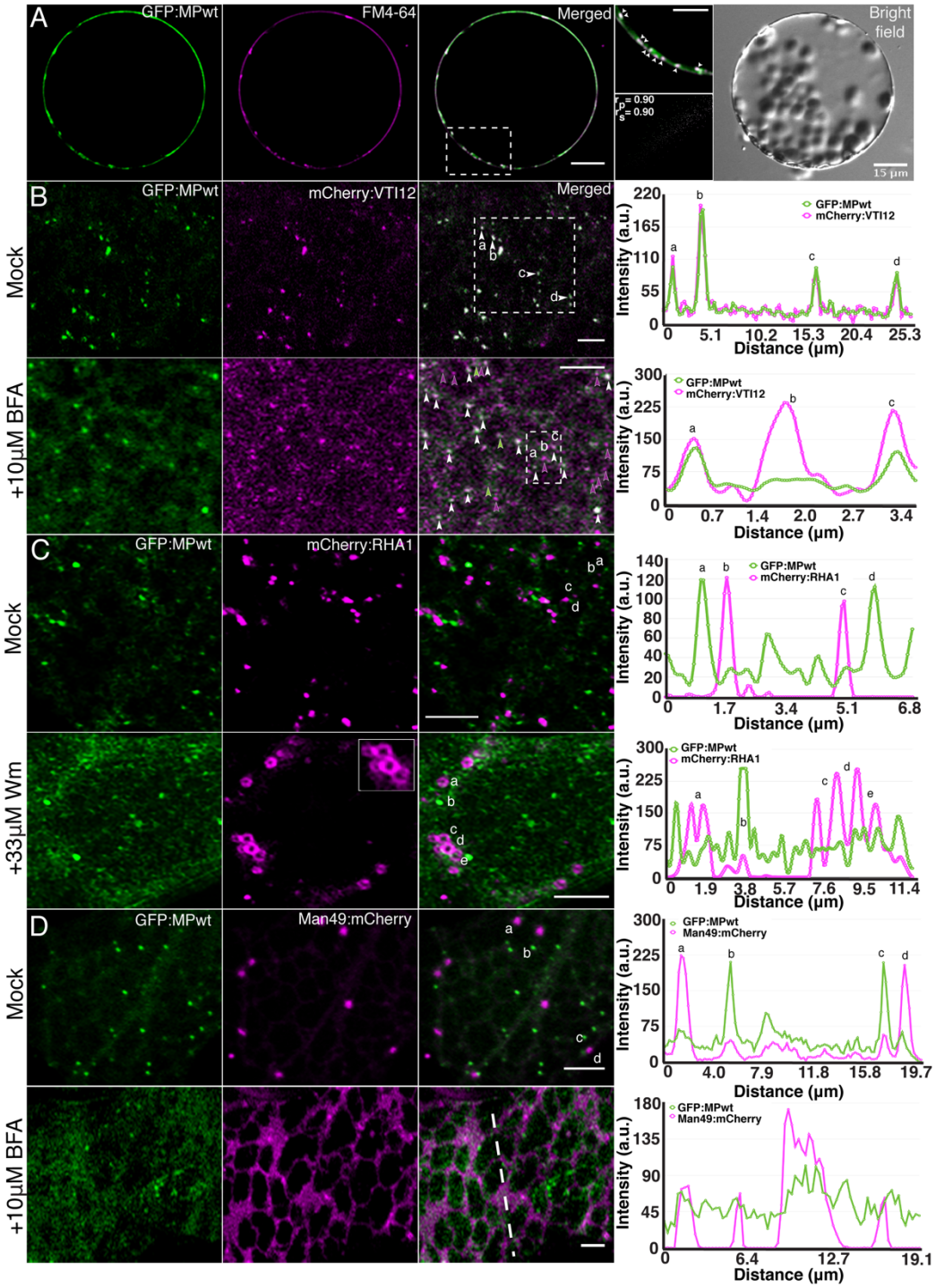

Figure 1. OuMV MP localizes to the TGN/EE, but not to the MVB/PVC or Golgi. (A) *N. benthamiana* protoplasts expressing OuMV GFP:MPwt (green) with CP and RdRP. Protoplasts were stained with FM4-64, an endocytic tracer (magenta). A selected region (white rectangle) was analyzed to show the colocalization of MP-labeled

punctate structures (arrowheads) with FM4-64. The extent of colocalization was quantified using the PSC plugin in ImageJ. rp, linear Pearson correlation coefficient; rs, nonlinear Spearman's rank correlation coefficient. Images represent single optical planes. Scale bars, 15 µm, 10 µm (magnified region). (B-D) *N. benthamiana* epidermal cells expressing GFP:MPwt (green) with RdRp and CP, and organelle markers (magenta), (B) mCherry:VTI12 (TGN/EE), (C) mCherry:RHA1 (MVB/PVC) and (D) Man49:mCherry (Golgi). Cells were treated with 10 µM BFA (B and D, bottom panel) or 33 µM wortmannin (C, bottom panel) for 1h. White arrowheads indicate colocalized spots, green and magenta arrowheads denote individual GFP:MPwt and mCherry:VTI12 spots respectively. Images were taken at 66 hpi. Panels represent maximum intensity Z projections. A selected region was analyzed to show the intensity profile generated by ImageJ. Scale bars, 5 µm.

Figure 2.

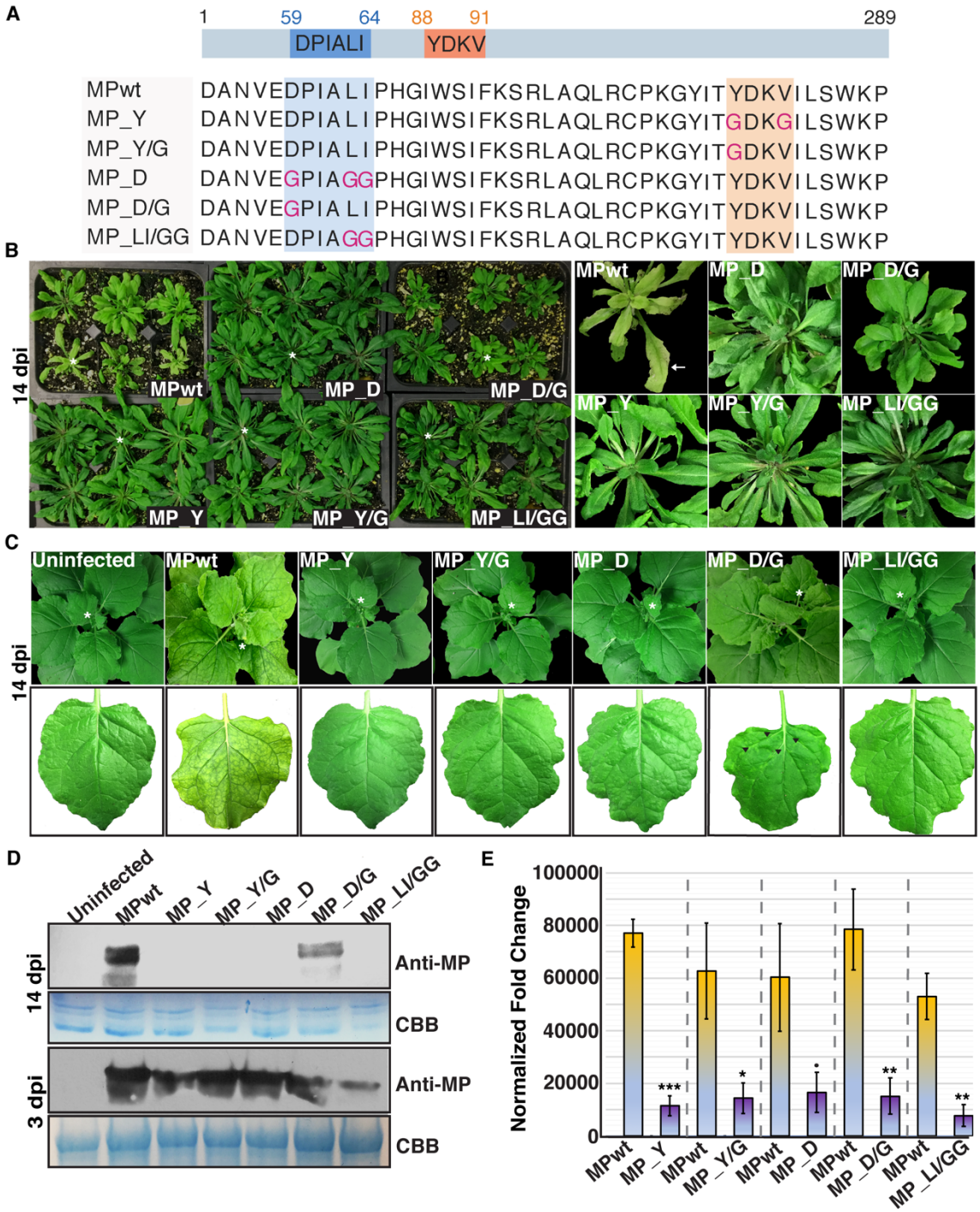

Figure 2. Loss of infectivity and reduced viral replication of OuMV carrying Y and LL motif MP mutants. (A) Schematic representation of constructs used in this study. Boxes indicate Y and LL motifs, and mutated sites are shown in pink. The illustration was created with BioRender.com. (B-C) Viral symptoms on Arabidopsis and *N. benthamiana* agroinfiltrated with pGC-RNA1 (RdRp), pGC-RNA3 (CP), and pGC-RNA2

(MP) with indicated mutations, or sterile water (mock) at 14 dpi. White asterisks denote leaves shown in close-up images. Black arrowheads indicate mosaic symptoms on *N. benthamiana* infected with OuMV carrying MP_D/G. (D) Western blot analysis of agroinfiltrated leaves at 3 dpi (bottom panel) and upper uninoculated leaves at 14 dpi (top panel). CBB: Coomassie Brilliant Blue, loading control. (E) Replication assay of OuMV carrying Y and LL motif MP mutants at 48 hpi. Two leaf spots from 3 leaves were pooled for each sample at 24 hpi and 48 hpi. The qPCR was performed in duplicates. The $2^{-\Delta\Delta CT}$ method was used to asses fold changes in replication of wild-type and mutants. The data was normalized first using 18S ribosomal RNA, and then a wild-type control at 24 hpi showing the lowest expression. Bar graph represents normalized fold changes (mean±SE, n=4). ˙, $P < 0.1$; *, $P < 0.05$; **$P < 0.01$; ***, $P < 0.001$ by ANOVA.

Figure 3.

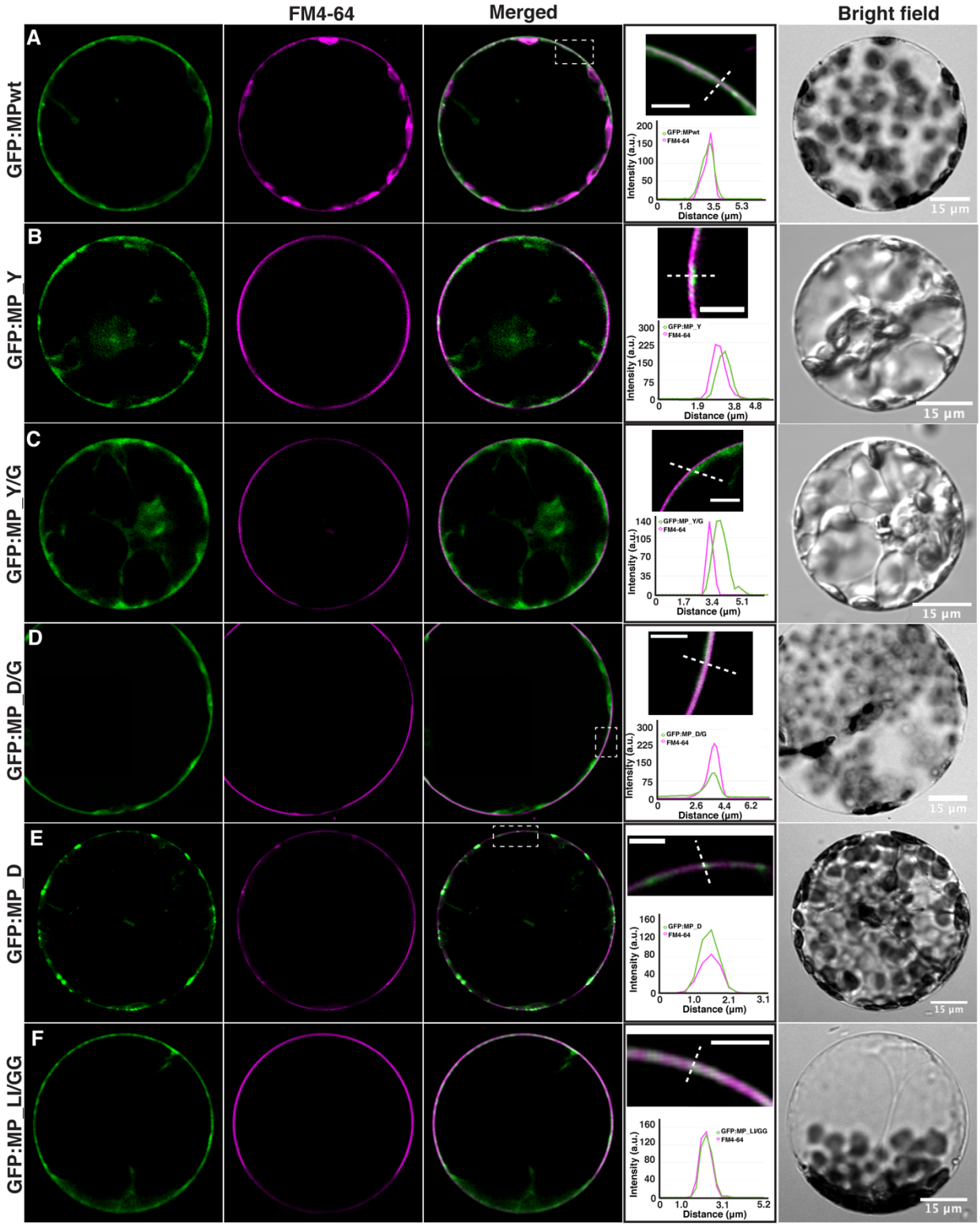

Figure 3. Plasma membrane localization of MP mutants. *N. benthamiana* protoplasts expressing (A) GFP:MPwt or GFP:MP mutants, (B) GFP:MP_Y, (C) GFP:MP_Y/G, (D) GFP:MP_D/G, (E) GFP:MP_D and (F) GFP:MP_LI/GG along with RdRp and CP.

Protoplasts were stained with FM4-64, a plasma membrane marker (magenta). Selected regions (white rectangles) show the intensity profile of the diagonal line were generated by ImageJ. Images represent single optical planes. Scale bar, 5 µm (magnified region).

Figure 4.

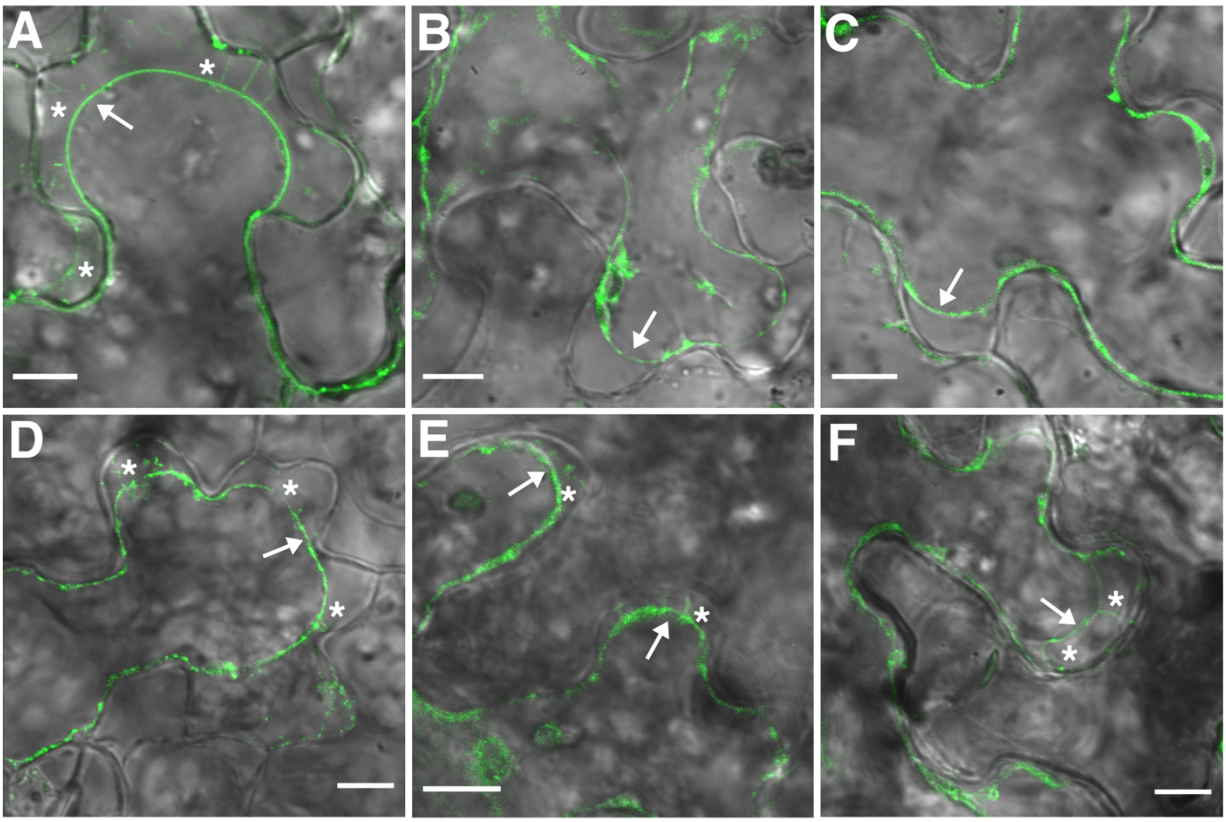

Figure 4. LL motif MP mutants are targeted to the plasma membrane. *N.benthamiana* epidermal cells expressing (A) GFP:MPwt or GFP:MP mutants, (B) GFP:MP_Y, (C) GFP:MP_Y/G, (D) GFP:MP_D/G, (E) GFP:MP_D and (F) GFP:MP_LI/GG along with RdRp and CP. were plasmolyzed with 1M mannitol. Arrows show the retracted plasma membrane and astrisks denote Hechtian stands. Images were taken at 62-66 hpi and represent single optical planes. Scale bar, 10 µm.

Figure 5.

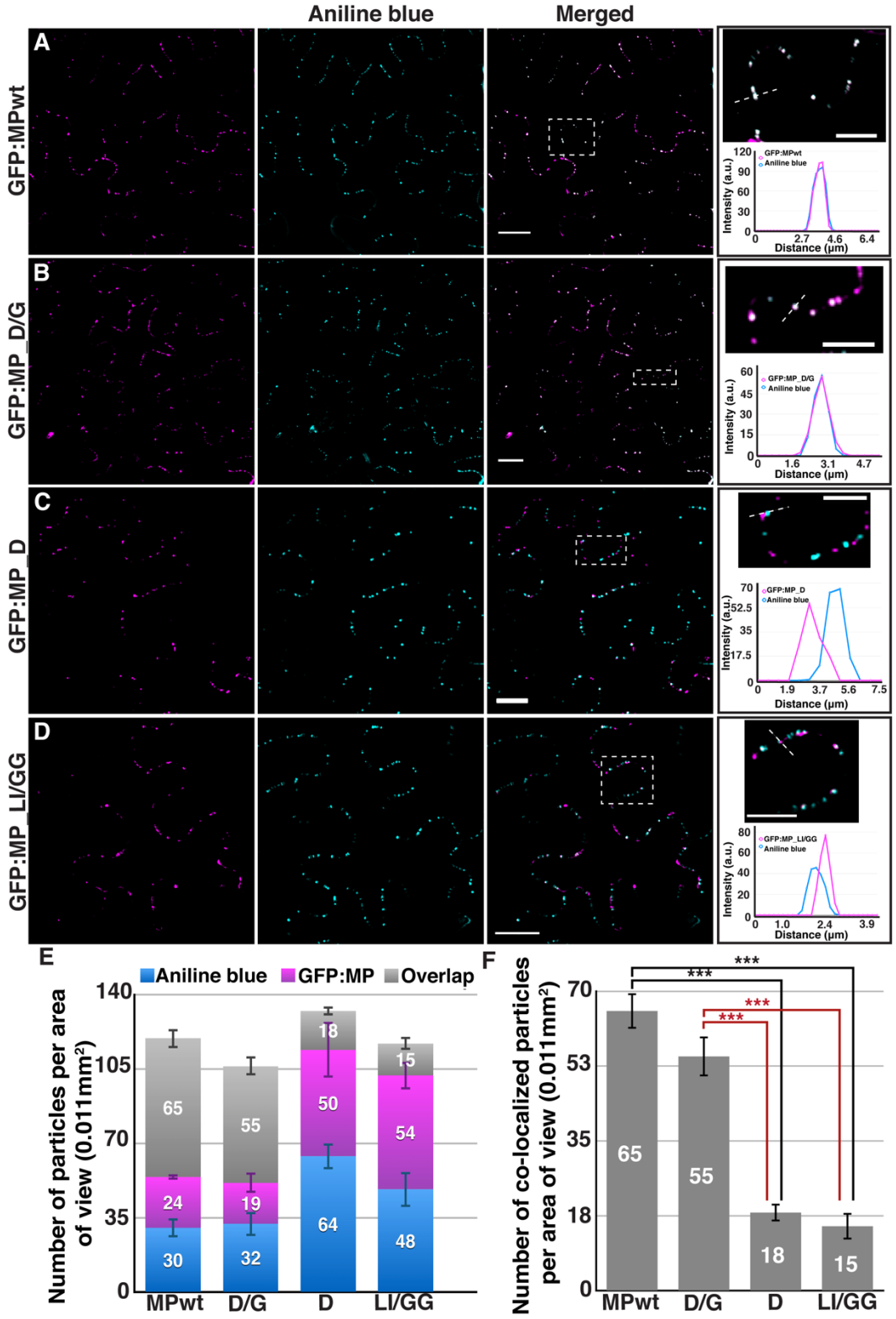

Figure 5. Movement deficient LL motif MP mutants do not localize to callose deposits. N. *benthamiana* epidermal cells expressing (A) GFP:MPwt or GFP:MP

mutants, (B) GFP:MP_D/G, (C) GFP:MP_D, and (D) GFP:MP_LI/GG (magenta) with RdRp and CP. Aniline blue was used to mark callose deposits (cyan). Selected regions (white rectangles) show the intensity profile of the diagonal line generated from images that were adjusted to a lower intensity by ImageJ. Images represent single optical planes. Scale bar, 20µm, 10 µm (magnified region). (E) The quantification of callose deposits (blue), punctate structures labeled by OuMV GFP:MPwt or GFP:MP mutants (magenta), and co-localized particles (gray) per area of view. The particles were counted using the ComDet v.0.4.1 plugin in ImageJ. At least 6 areas of view were examined ($n \geq 6$) and the total number of counted particles for each sample is more than 700. Error bars indicate standard error of the mean. (F) The statistical analysis of co-localized particles in (E). Bar graph represents PD-localized OuMV GFP:MPwt or GFP:MP mutants per area of view (mean±SE, $n \geq 6$). ***, $P < 0.001$ by ANOVA, followed by Tukey's HSD.

Figure 6.

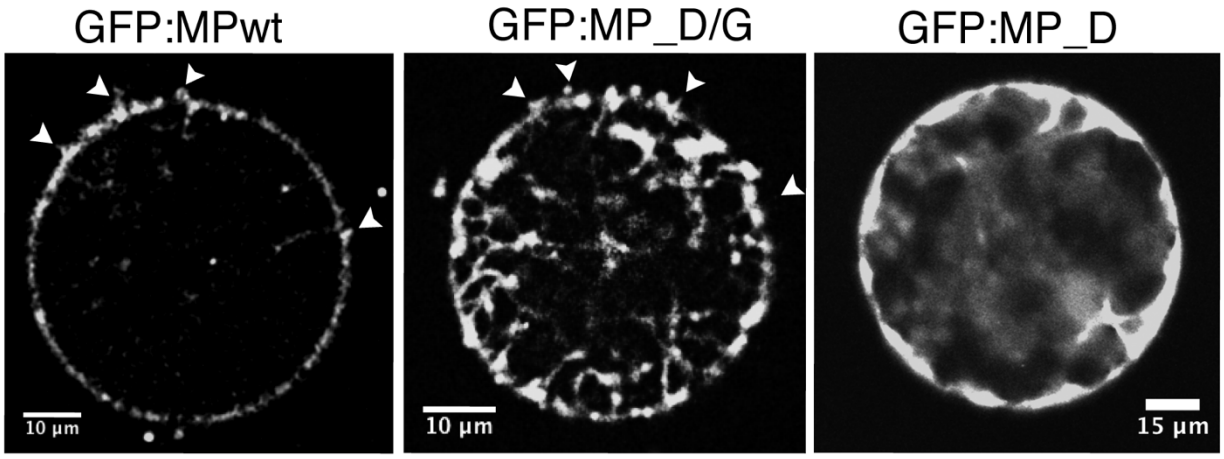

Figure 6. Movement deficient LL motif MP mutant, MP_D, does not form tubules. Confocal microscopy images of *N. benthamiana* protoplasts expressing GFP:MPwt or LL motif MP mutants, GFP:MP_D/G and GFP:MP_D. Images represent single optical planes. Arrowheads indicate tubules/protrusions. Images are overexposed to show tubules/protrusions.

Figure 7.

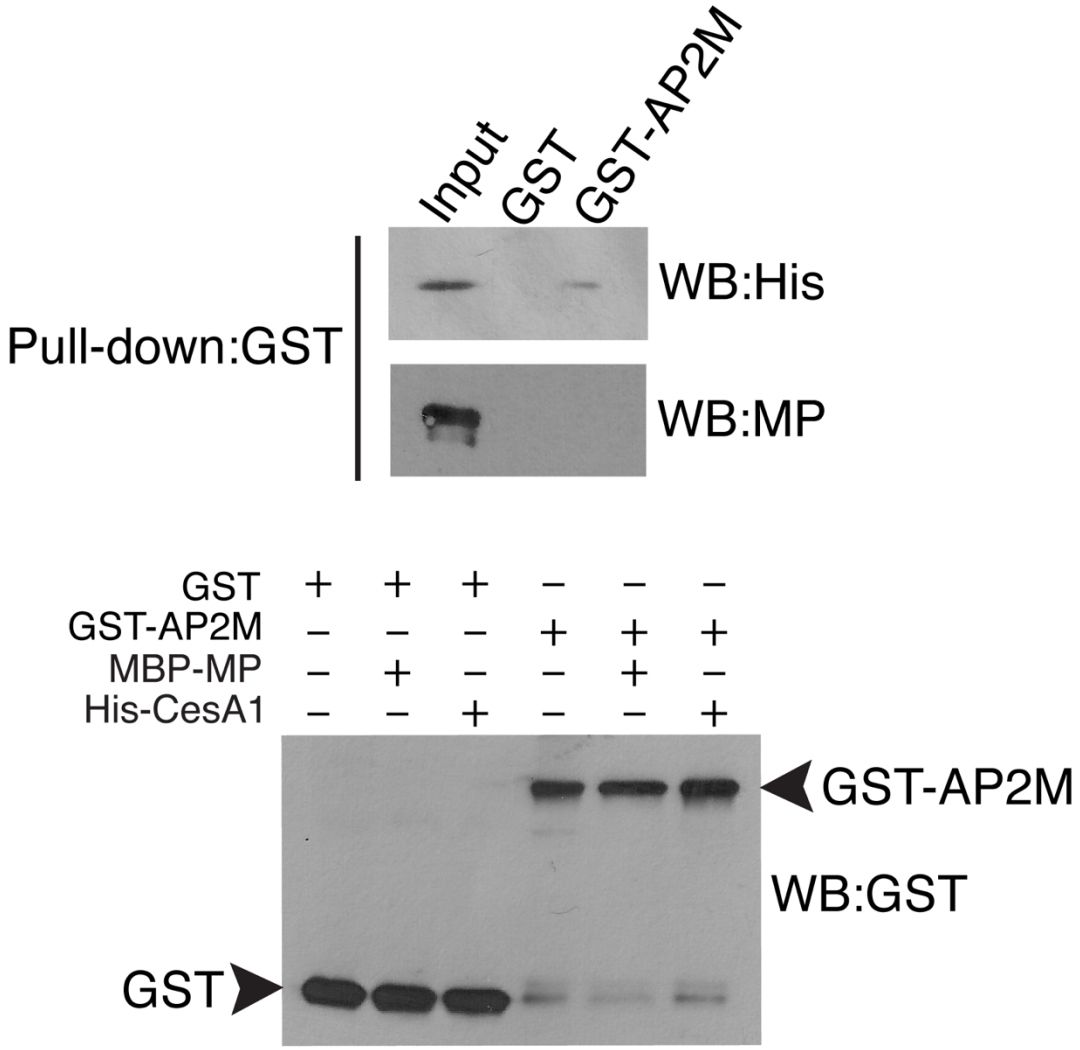

Figure 7. OuMV MP does not directly interact with AP2M. Pull-down of GST-AP2M-MHD and MBP-MP was performed using GST-Trap. His-CesA1 was used as a positive control. Resin-bound GST or GST-AP2M-MHD (bottom panel) was incubated with purified His-CesA1 (top panel, lane 1: Input) or MBP-MP (middle panel, lane 1: Input). His-CesA1 interacts with GST-AP2M-MHD, but not with GST (top panel, lane 2: GST with His-CesA1 (negative control); lane 3: GST-AP2M-MHD with His-CesA1 (positive control)). Under same conditions, MBP-MP was not able to bind GST-AP2M-MHD (Middle panel, lane 2: GST with MBP-MP (negative control); lane 3: GST-AP2M-MHD with MBP-MP). Proteins were immunoblotted for GST, 6xHis tag, and MP.

Figure 8.

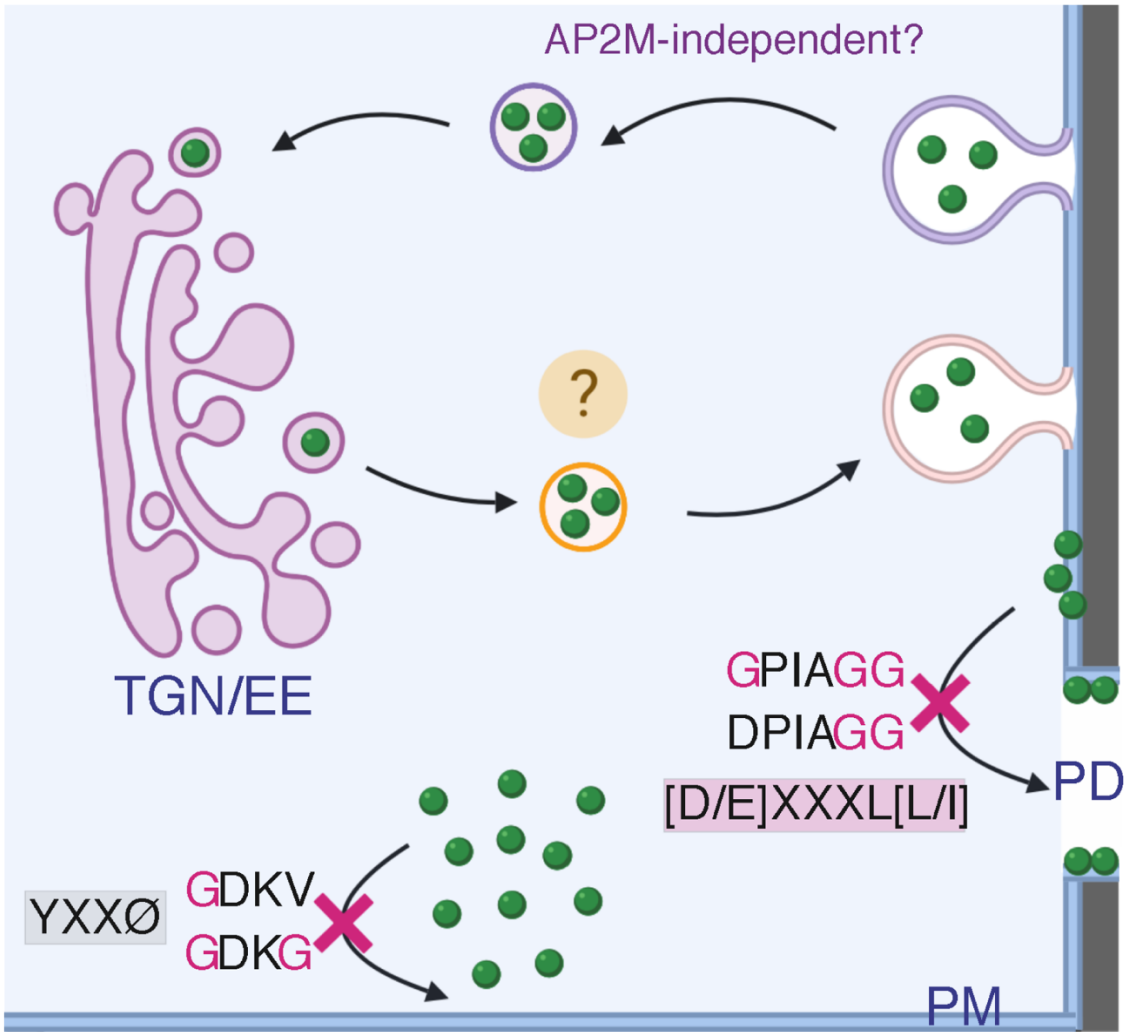

Figure 8. Working model for intracellular trafficking of OuMV MP. The MP (green) is targeted to the plasma membrane via an unknown mechanism. It is retrieved from the plasma membrane (purple) and transported to the TGN (light purple). AP2M is not directly involved in this process. From the TGN, the MP is recycled back to the plasma membrane (orange). The Y motif (gray box) possibly acts as a structural motif rather than a functional internalization motif, whereas the LL motif (pink box) is required for correct plasmodesmal targeting of MP. TGN/EE, trans-Golgi network/ early endosome; PM, plasma membrane; PD, plasmodesmata. The model was created with BioRender.com

Table 1.

Table 1. Infectivity assays of OuMV carrying MPwt or MP mutants in *N.benthamiana* and Arabidopsis[a]

Virus	Systemically infected plants/ total inoculated plants					
	N.benthamiana			**Arabidopsis (Col-0)**		
	Exp. 1	Exp. 2	Exp. 3	Exp.1	Exp. 2	Exp. 3
OuMV-MPwt	6/6	6/6	6/6	8/12	9/12	7/12
OuMV-MP_Y	0/6	0/6	0/6	0/12	0/12	0/12
OuMV-MP_D	0/6	0/6	0/6	0/12	0/11	1*/12
OuMV-MP_Y/G	0/6	0/6	0/6	0/12	0/12	0/12
OuMV-MP_D/G	6/6	5/5	6/6	6/12	8/12	6/12
OuMV-MP_LI/GG	0/6	0/6	0/6	0/12	0/12	0/12

[a]OuMV: *Ourmia melon virus*
*Revertant

Table 2.

Table 2. Systemic infection by OuMV in Arabidopsis Col-0 (wt), *ap2m-1* mutant and AP2M-YFP complementation line at 14 dpi

	Systemically infected plants/ total inoculated plants
Col-0 (wt)	7/12
ap2m-1	7/12
AP2M-YFP/*ap2m-1*	6/12

Table 3.

Table 3. Infectivity, replication, and subcellular localization of Y and LL motif mutants

	Systemic infection	Replication	Subcellular localization			Tubule formation
			Cytoplasmic puncta	PM	PD	
MPwt	**+**	**wt**	**+ (TGN/endosomes and occasional immobile)**	**+**	**+**	**+**
MP_Y	**-**	**decreased**	**-**	**-**	**-**	**N/A**
MP_ Y/G	**-**	**decreased**	**- (a few, immobile)**	**-**	**-**	**N/A**
MP_D	**-**	**decreased**	**+ (mobile, occasional immobile)**	**+**	**-**	**-**
MP_D/G	**+**	**decreased**	**+ (mobile, occasional immobile)**	**+**	**+**	**+**
MP_LI/GG	**-**	**decreased**	**+ (mobile, occasional immobile)**	**+**	**-**	**-**

PM: plasma membrane, PD: plasmodesmata